International Journal of Minerals, Metallurgy and Materials
Volume 25, Number 10, October 2018, Page 1166
http://doi.org/10.1007/s12613-018-1668-6

Microstructure evolution of a recycled Al–Fe–Si–Cu alloy processed by tube channel pressing

M.H. Farshidi[1)], *M. Rifai*[2)], *and H. Miyamoto*[2)]

1) Department of Materials Science and Metallurgical Engineering, Ferdowsi University of Mashhad, Azadi Square, Mashhad 9177948974, Iran
2) Department of Mechanical Engineering, Doshisha University, Kyotanabe city, Kyoto 610-0394, Japan
(Received: 18 January 2018; revised: 25 May 2018; accepted: 27 May 2018)

Abstract: Although excellent recyclability is one of the advantages of Al alloys, a recycling process can reduce different properties of these alloys by adding coarse AlFeSi particles into the alloys' microstructures. One of the well-known methods for modifying the microstructure of metallic materials is the imposition of severe plastic deformation (SPD). Nevertheless, the microstructure evolutions of recycled Al alloys containing extraordinary fractions of AlFeSi particles during SPD processing have seldom been considered. The aim of the present work is to study the microstructure evolution of a recycled Al–Fe–Si–Cu alloy during SPD processing. For this purpose, tubular specimens of the mentioned alloy were subjected to different numbers of passes of a recently developed SPD process called tube channel pressing (TCP); their microstructures were then studied using different techniques. The results show that coarse AlFeSi particles are fragmented into finer particles after processing by TCP. However, decomposition and dissolution of AlFeSi particles through TCP processing are negligible. In addition, TCP processing results in an increase in hardness of the alloy, which is attributed to the refinement of grains, to an increase of the dislocation density, and to the fragmentation of AlFeSi particles.

Keywords: AlFeSi; intermetallic particle; severe plastic deformation; microstructure; tube channel pressing

1. Introduction

Al alloys are widely used in different industries not only because of their well-known specifications such as high corrosion resistance, low density, and reasonable mechanical properties but also because of their excellent recyclability. As an illustration, approximately 40%–60% of Al products have been estimated to be fabricated from recycled stocks [1–2]. However, a recycling process may contaminate the composition of Al alloys through addition of different impurities such as Fe and Si [3–4]. These impurities adversely affect various properties of Al alloys because they induce the formation of insoluble AlFeSi intermetallic particles. For example, these particles accelerate the fracture of Al alloys during forming processes because they function as stress concentration sites [3–5]. In addition, these particles accelerate the pitting corrosion rate of Al alloys by activating selective corrosion mechanisms [6–7]. Although different methods have been proposed for eliminating Fe and Si from recycled Al alloys, these methods are often complex, ineffective, or expensive [3–4]. In addition, coarsening of the intermetallic particles has been speculated to intensify their adverse effects on the properties of Al alloys [5–7]. Therefore, we propose that the properties of a recycled Al alloy can be improved through the reduction of the dimensions of their intermetallic particles. One of the well-known methods for refining the microstructure of metals is imposition of severe plastic deformation (SPD) [8–10]. However, the literature contains few studies focused on the effects of the SPD processing on the evolution of the microstructure and variation of the properties of recycled Al alloys with extraordinary concentrations of Fe and Si.

The aim of the present work is to investigate the evolution of the microstructure of a recycled Al alloy during SPD processing. Because SPD processing of tubes is attractive for industrial applications [8], a recently developed SPD process for tubes called tube channel pressing (TCP) was applied for this purpose. The evolution of the microstruc-

Corresponding author: M.H. Farshidi E-mail: farshidi@um.ac.ir

ture of the alloy was then studied using scanning electron microscopy (SEM) and X-ray diffraction (XRD) techniques.

2. Process, materials, and methods

TCP has been recently developed for SPD processing of tubes. In this process, the tube is strained through passing a bottleneck region, which causes multiple stages of shear straining in addition to two stages of hoop straining. Fig. 1(a) illustrates a new geometry for the TCP process used in this work. Using a finite element (FE) simulation, the average plastic strain imposed on the tube wall through the applied geometry of TCP is evaluated to be approximately 1.3. Figs. 1(b) and 1(c) show the manufactured TCP die and the processed specimen, respectively. Additional details about the process and the applied FE simulation are presented elsewhere [11–14].

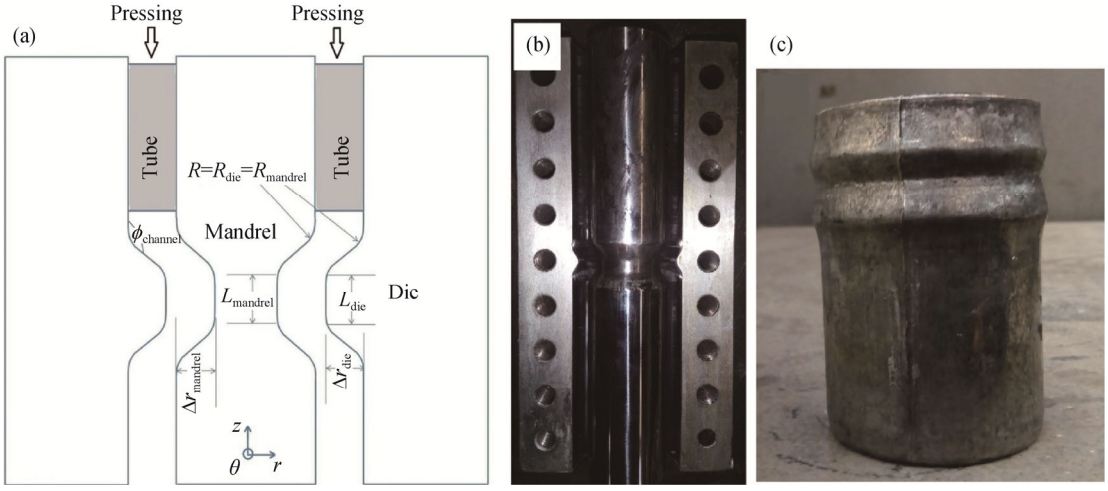

Fig. 1. Schematic of the new geometry of the TCP process (a), the manufactured die and mandrel of the TCP process for the new geometry (b), and a TCP-processed tube (c).

A recycled Al tube was received in wrought form. The inner and outer diameters of the tube were 44.4 and 50.8 mm, respectively. The chemical composition of the recycled Al tube was evaluated using optical emission spectrometry to be Al–1.7Fe–0.9Si–0.5Cu. The received tube was cut into different specimens, which were subsequently annealed at 753 K for 45 min. Afterwards, they were subjected to zero, one, four, and eight passes of TCP at room temperature using a strain rate of approximately 0.1 s^{-1}. This process resulted in the imposition of different plastic strains of 0, 1.3, 5.2, and 10.4, respectively. After TCP processing, a Vickers hardness test was performed in the r–θ plane of the tubular specimens using an indentation load of 98 N.

The XRD patterns of TCP-processed specimens were recorded at an interval step angle of 0.02° using Cu K_α X-rays with a wavelength of 0.154 nm. The range of the diffraction angles was 10° and 50°. Considering broadening of the integral breadth of Al peaks, the Williamson–Hall approach was used to evaluate the dislocation density of TCP-processed specimens [15–16]. In addition, two different groups of samples were prepared for SEM studies. The first group was prepared by conventional polishing and etching and was used to characterize AlFeSi particles. The second group was prepared by ion polishing and was used for electron backscattering diffraction (EBSD) studies of the Al matrix on a JEOL JSM-7001F scanning electron microscope. Different magnifications from 200× to 5000× were used for SEM and SEM/EBSD studies, whereas multiple step sizes from 0.1 to 2.5 μm were applied to obtain EBSD maps. In addition, the INCA^{TM} 4.09 software was used to interpret EBSD maps.

3. Results and discussion

3.1. Effect of TCP processing on intermetallic particles

Fig. 2 compares XRD patterns of the used alloy before and after TCP processing. Different peaks related to the Al matrix and to α-AlFeSi particles are observed in the XRD patterns. Notably, peaks related to α-AlFeSi particles remain even after eight passes of TCP, which implies that these particles are stable during SPD processing.

Fig. 3 compares the morphology, dimensions, and distribution of AlFeSi intermetallic particles in the microstructure of the used alloy before and after TCP processing. As shown before, these particles usually appear in two different elongated and faceted morphologies [17–19]. As evident in Figs. 3(a)–3(e), different AlFeSi particles can be traced in the

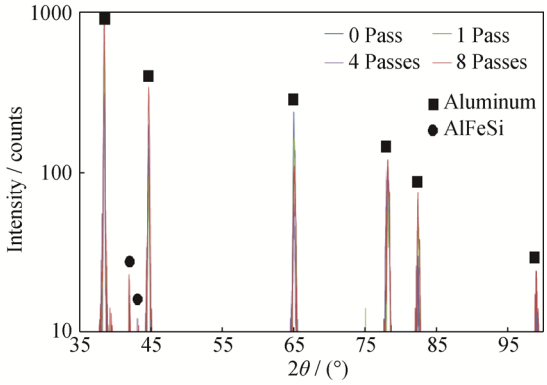

Fig. 2. XRD patterns of the alloy after different numbers of passes of TCP.

microstructure of the alloy before and after TCP processing. The chemical compositions of differently numbered particles shown in Fig. 3 are presented in Table 1. As can be traced in this table, the chemical composition of these particles is approximately 33wt% Fe, 6wt% Si, and 57wt% Al. This chemical composition is very similar to that of α-AlFeSi (Al_8Fe_2Si). As shown in Fig. 3(a), three groups of AlFeSi particles can be traced in the microstructure of the alloy before TCP processing:

(1) Coarse-faceted particles with sizes between 5 and 10 μm;

(2) Elongated particles with lengths of 5 to 10 μm and a width of about 1 μm;

(3) Fine particles smaller than 5 μm.

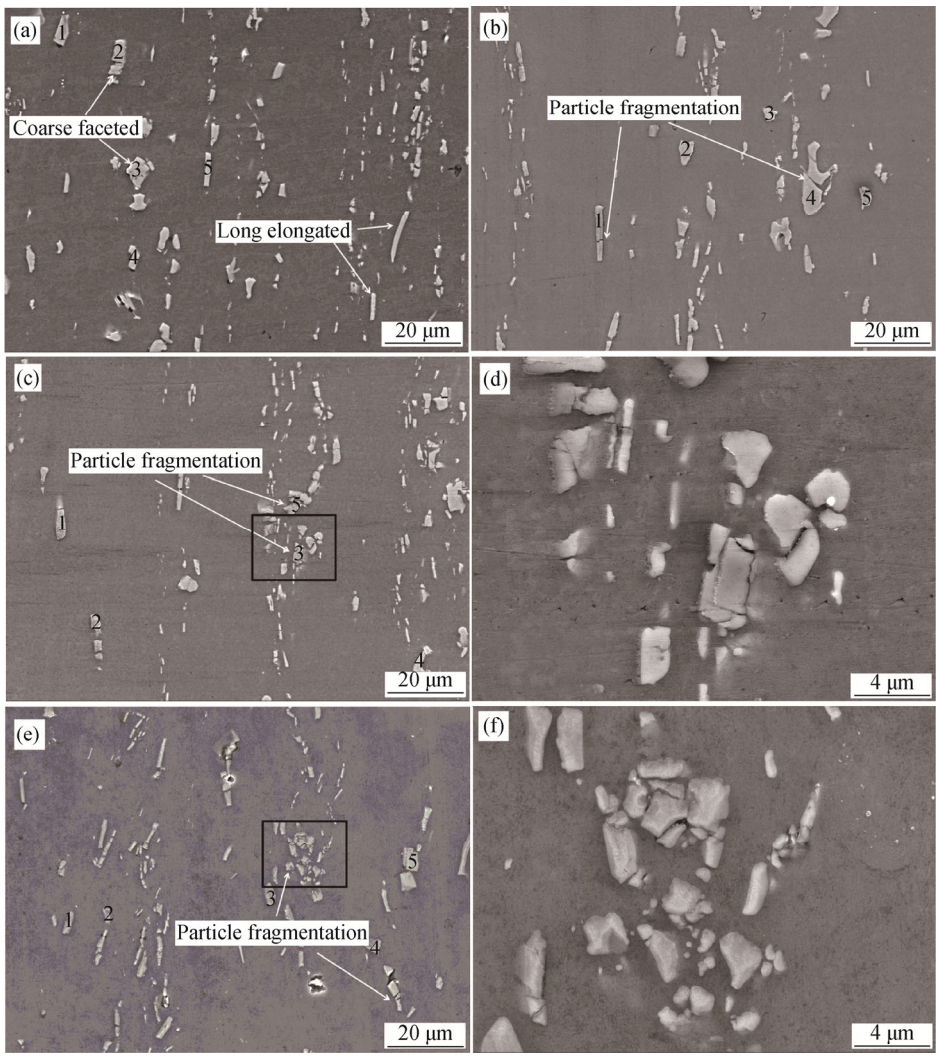

Fig. 3. Morphology and size distribution of the intermetallic particles after (a) 0, (b) 1, (c,d) 4, and (e,f) 8 passes of TCP. Black rectangles shown in (c) and (e) indicate the similar areas of (d) and (f), respectively.

As shown in Fig. 3(b), the morphology and dimensions of AlFeSi intermetallic particles after one pass of TCP are similar to those before TCP processing. However, slight evidences of fragmentation of coarse-faceted and elongated particles can be traced after one TCP pass. This fragmentation of particles is more obvious after four TCP passes, as

shown in Figs. 3(c) and 3(d). Consistently, almost all of the coarse-faceted and elongated particles are fragmented into fine particles after eight TCP passes, as shown in Figs. 3(e) and 3(f). Similar to the results observed in this study for AlFeSi particles, fragmentation of other particles inside Al alloys subjected to SPD processing has been reported. This fragmentation is caused by the concentration of stress on the particles during SPD processing mainly occurring via pile-up of dislocations behind them through deformation [20–22].

Table 1. Chemical compositions of different intermetallic particles shown in Fig. 3 wt%

Number of passes	Particle No.	Composition			
		Al	Si	Fe	Cu
0	1	59.0	5.2	31.9	3.6
	2	64.3	4.9	27.6	3.2
	3	54.0	6.0	35.4	4.6
	4	59.0	5.5	32.0	3.5
	5	63.5	5.1	27.9	3.5
	Average	59.96	5.34	30.96	3.74
1	1	56.1	5.6	33.9	4.4
	2	54.7	5.8	34.9	4.6
	3	58.6	5.4	32.7	3.3
	4	53.6	6.2	36.0	4.2
	5	53.1	5.5	37.8	3.5
	Average	55.2	5.7	35.1	4.0
4	1	53.6	6.2	35.3	4.9
	2	52.6	6.2	36.2	5.1
	3	54.3	6.2	35.0	4.5
	4	65.2	4.3	27.6	2.9
	5	72.0	4.0	21.4	2.5
	Average	59.5	5.4	31.1	4.0
8	1	62.4	5.6	28.5	3.6
	2	57.8	5.7	32.8	3.7
	3	54.6	6.0	34.5	4.9
	4	55.2	6.3	34.3	4.3
	5	54.5	5.9	35.2	4.3
	Average	56.9	5.9	33.1	4.1

Fig. 4 compares variations in the chemical compositions of different specimens along the selected line shown in red. As illustrated in Fig. 4(a), the content of alloying elements in the Al matrix is negligible before TCP processing. Also, the alteration of chemical composition between the intermetallic particles and the Al matrix is very rapid. These results imply a complete separation of alloying elements from the Al matrix due to the formation of AlFeSi intermetallic particles. Similar to what was observed for an unprocessed specimen, the content of alloying elements in the Al matrix was negligible after one, four, and eight passes of TCP, as shown in Figs. 4(b)–4(d). In addition, the rapid alteration of chemical composition between the intermetallic particles and the Al matrix remained even after eight passes of TCP. These results suggest that decomposition and dissolution of AlFeSi intermetallic particles through TCP processing are negligible. Nonetheless, SPD has been reported to cause decomposition and dissolution of other intermetallic particles such as $CuAl_2$ and $MgZn_2$ [22–23]. To explain this difference, we refer to the chemical stability of AlFeSi particles, which prevents its decomposition and dissolution by SPD processing. As an explanation of this behavior, whereas the enthalpy of formation of $CuAl_2$ and $MgZn_2$ has been reported to be approximately −13 and −14 kJ/mol, respectively, the enthalpy of formation of α-AlFeSi is approximately −26 kJ/mol [24–26].

3.2. Effect of TCP processing on the aluminum matrix

Table 2 illustrates variations in the dislocation density of the alloy subjected to TCP processing. The dislocation density of the alloy impressively increases after one pass of TCP and then remains nearly constant with additional passes of TCP. Similarly, a rapid increase of the dislocation density by imposition of a relatively small plastic strain (~1) and a successive saturation of the dislocation density with imposition of greater plastic strains have been reported for other dilute Al alloys subjected to SPD processing [27–28]. To explain this phenomenon, we note that dilute Al alloys regularly undergo dynamic recovery during SPD processing even at room temperature. Therefore, the increase in dislocation density of these alloys through SPD processing becomes saturated because of the appearance of an equilibrium between dislocation multiplication caused by plastic deformation and dislocation annihilation induced by dynamic recovery [8,17].

Fig. 5 compares EBSD maps of the alloy sample before and after TCP processing. Fig. 5(a) shows that the grain size of the Al matrix before the process is greater than 250 μm. After one pass of TCP processing, initial coarse grains are broken into impressively finer grains, as illustrated in Fig. 5(b). The overall grain size after one pass of TCP processing is evaluated to be equal to 2.26 μm. As shown in Fig. 5(c), the overall grain size after four passes of TCP processing is slightly lower compared to that observed after one pass of TCP processing. Nevertheless, the overall grain size after eight passes of TCP processing is similar to that after four passes of TCP processing, as illustrated in Fig. 5(d). The overall grain sizes after four and eight passes of TCP processing are 1.43 and 1.39 μm, respectively. These results imply saturation of grain refinement of the used alloy through TCP processing.

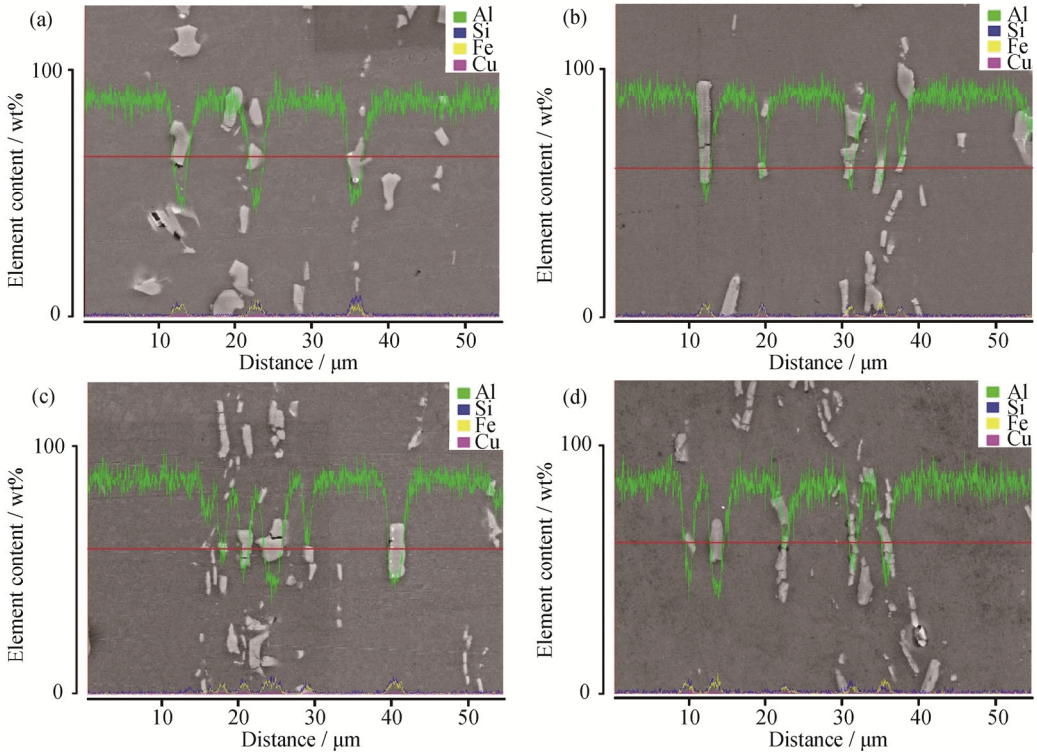

Fig. 4. Variation of the chemical composition of the alloy along a selected line shown in red after (a) 0, (b) 1, (c) 4, and (d) 8 passes of TCP.

Table 2. Evaluated dislocation densities after different numbers of passes of TCP m^{-2}

Number of passes	Dislocation density
0	$\approx 10^{12}$
1	$(3.6 \pm 1.1) \times 10^{14}$
4	$(5.5 \pm 1.3) \times 10^{14}$
8	$(3.8 \pm 0.2) \times 10^{14}$

The saturation of grain refinement for other dilute Al alloys subjected to SPD processing has been previously reported [16,29–30]. The grain refinement of dilute Al alloys through SPD processing is speculated to occur because of the occurrence of continuous dynamic recrystallization (CDRX). CDRX, sometimes known as extended recovery, occurs because of the initial multiplication of dislocations, migration

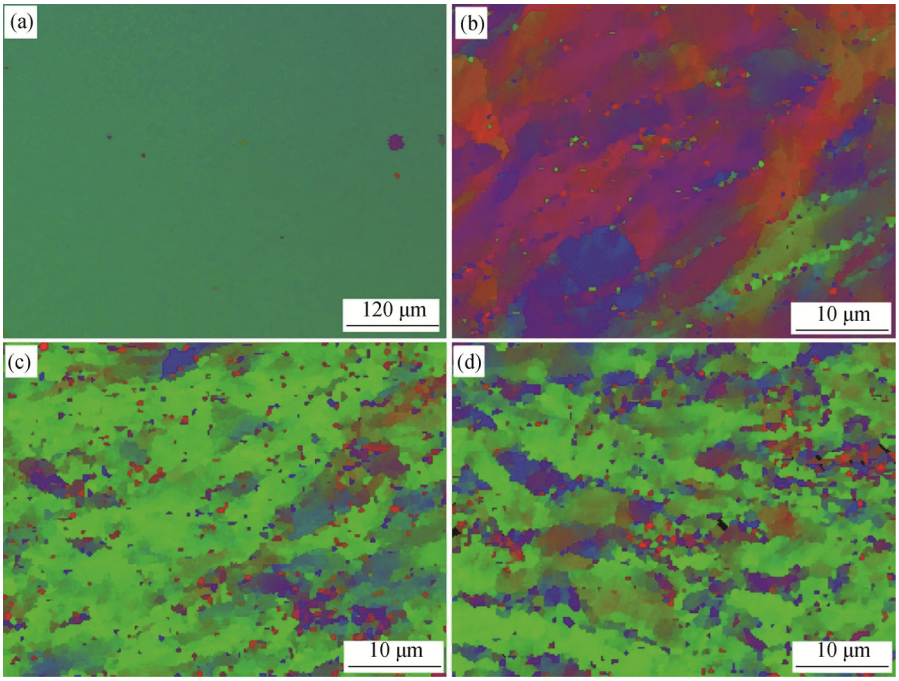

Fig. 5. EBSD maps of the alloy after (a) 0, (b) 1, (c) 4, and (d) 8 passes of TCP.

of dislocations to form dislocation cell walls/low-angle grain boundaries, and further evolution of the low-angle grain boundaries to high-angle grain boundaries [29–30]. Also, the saturation of grain refinement during SPD processing has been attributed to the diffusive accommodation of dislocations through grain boundaries instead of through cell formation after the grain size reaches its lowermost critical amount [8].

3.3. Variation of hardness through TCP processing

As shown in Table 3, an extensive increase in hardness of the used alloy occurs after one pass of TCP. This extensive increase in hardness is mainly attributed to a reduction of the grain size as well as to an increase in dislocation density; these effects are the main strengthening mechanisms of dilute Al alloys subjected to SPD processing [29,31]. Compared with this extensive increase in hardness of the alloy, the increase in hardness induced by additional TCP passes is small. This effect is due to an increase of the limited dislocation density and to grain-size reduction through further TCP passes, as previously mentioned. However, the question arises: If the dislocation density and the grain size of the alloy remain almost constant after four TCP passes, why does the hardness increase after eight TCP passes? To answer this question, we refer to the fragmentation of AlFeSi particles through TCP processing, especially after eight passes. Note that the fragmentation of particles causes the appearance of an extra number of finer particles, which results in an additional strengthening effect according to the Orowan mechanism [29,32–33].

Table 3. Hardness of the used alloy after imposition of different passes of TCP

Number of passes	Vickers hardness
0	47.9 ± 2.0
1	78.0 ± 1.2
4	81.0 ± 2.5
8	88.9 ± 0.3

4. Conclusions

(1) TCP processing caused fragmentation of AlFeSi particles present in the microstructure of the Al–1.7Fe–0.9Si–0.5Cu alloy. Nearly all of the coarse AlFeSi particles were fragmented after eight passes of TCP (an equivalent plastic strain of about 10).

(2) AlFeSi particles remaining in the microstructure of the used alloy did not decompose/dissolve into the Al matrix during TCP processing because of their chemical stability.

(3) The increase in hardness through TCP processing occurred not only because of the increase in dislocation density and the reduction of grain size, but also because of the fragmentation of AlFeSi particles.

Acknowledgements

The corresponding author wishes to thank the research board of Ferdowsi University of Mashhad (FUM) for the financial support and the provision of research facilities used in this work through grant number 2/43989. The authors also thank Doshisha University for the provision of research facilities used in this work.

References

[1] J.Y. Hwang, X. Huang, and Z. Xu, Recovery of metals from aluminum dross and salt cake, *J. Miner. Mater. Charact. Eng.*, 5(2006), No. 1, p. 47.

[2] J. Blomberg and P. Söderholm, The economics of secondary aluminium supply: An econometric analysis based on European data, *Resour. Conserv. Recycl.*, 53(2009), No. 8, p. 455.

[3] C. Chen, J. Wang, D. Shu, P. Li, J. Xue, and B.D. Sun, A novel method to remove iron impurity from aluminum, *Mater. Trans.*, 52(2011), No. 8, p. 1629.

[4] H.L. de Moraes, J.R. de Oliveira, D.C.R. Espinosa, and J.A.S. Tenório, Removal of iron from molten recycled aluminum through intermediate phase filtration, *Mater. Trans.*, 47(2006), No. 7, p. 1731.

[5] Z. Ma, A.M. Samuel, H.W. Doty, S. Valtierra, and F.H. Samuel, Effect of Fe content on the fracture behaviour of Al–Si–Cu cast alloys, *Mater. Des.*, 57(2014), p. 366.

[6] B. Mingo, R. Arrabal, A. Pardo, E. Matykina, and P. Skeldon, 3D study of intermetallics and their effect on the corrosion morphology of rheocast aluminium alloy, *Mater. Charact.*, 112(2016), p. 122.

[7] R. Ambat, A.J. Davenport, G.M. Scamans, and A. Afseth, Effect of iron-containing intermetallic particles on the corrosion behaviour of aluminium, *Corros. Sci.*, 48(2006), No. 11, p. 3455.

[8] Y. Estrin and A. Vinogradov, Extreme grain refinement by severe plastic deformation: A wealth of challenging science, *Acta Mater.*, 61(2013), No. 3, p. 782.

[9] B. Hwang, S. Lee, Y.C. Kim, N.J. Kim, and D.H. Shin, Microstructural development of adiabatic shear bands in ultra-fine-grained low-carbon steels fabricated by equal channel angular pressing, *Mater. Sci. Eng. A*, 441(2006), No. 1-2, p. 308.

[10] T. Makhlouf, A. Rebhi, J.P. Couzinie, Y. Champion, and N. Njah, Microstructural evolution of a recycled aluminum alloy deformed by equal channel angular pressing process, *Int. J. Miner. Metall. Mater.*, 19(2012), No. 11, p. 1016.

[11] M.H. Farshidi and M. Kazeminezhad, Deformation behavior

of 6061 aluminum alloy through tube channel pressing: Severe plastic deformation, *J. Mater. Eng. Perform.*, 21(2012), No. 10, p. 2099.

[12] M.H. Farshidi and M. Kazeminezhad, The effects of die geometry in tube channel pressing: Severe plastic deformation, *Proc. Inst. Mech. Eng. Part L J. Mater. Des. Appl.*, 230(2016), No. 1, p. 263.

[13] M.H. Farshidi, Optimization of die geometry for tube channel pressing, *Iran. J. Mater. Form.*, 5(2018), p. 26.

[14] M.H. Farshidi, M. Kazeminezhad, and H. Miyamoto, Microstructure and mechanical properties of an Al–Mg–Si tube processed by severe plastic deformation and subsequent annealing, *Mater. Sci. Eng. A*, 640(2015), p. 42.

[15] G.K. Williamson and R.E. Smallman, III. Dislocation densities in some annealed and cold-worked metals from measurements on the X-ray debye-scherrer spectrum, *Philos. Mag.*, 1(1956,), No. 1, p. 34.

[16] W. Woo, T.S. Ungár, Z.L. Feng, E. Keink, and B. Clausen, X-ray and neutron diffraction measurements of dislocation density and subgrain size in a friction-stir-welded aluminum alloy, *Metall. Mater. Trans. A*, 41(2010), No. 5, p. 1210.

[17] H.W. Kim, S.B. Kang, N. Tsuji, and Y. Minamino, Elongation increase in ultra-fine grained Al–Fe–Si alloy sheets, *Acta Mater.*, 53(2005), No. 6, p. 1737.

[18] L. Sweet, S.M. Zhu, S.X. Gao, J.A. Taylor, and M.A. Easton, The effect of iron content on the iron-containing intermetallic phases in a cast 6060 aluminum alloy, *Metall. Mater. Trans. A*, 42(2011), No. 7, p. 1737.

[19] V. Raghavan, Al–Fe–Si (aluminum–iron–silicon), *J. Phase Equilib.*, 23(2002), No. 4, p. 362.

[20] K. Rhee, R. Lapovok, and P.F. Thoms, The influence of severe plastic deformation on the mechanical properties of AA6111, *JOM*, 57(2005), No. 5, p. 62.

[21] I. Gutierrez-Urrutia, M.A. Muñoz-Morris, and D.G. Morris, Contribution of microstructural parameters to strengthening in an ultrafine-grained Al-7% Si alloy processed by severe deformation, *Acta Mater.*, 55(2007), No. 4, p. 1319.

[22] C. Xu, M. Furukawa, Z. Horita, and T.G. Langdon, Influence of ECAP on precipitate distributions in a spray-cast aluminum alloy, *Acta Mater.*, 53(2005), No. 3, p. 749.

[23] W.H. Huang, Z.Y. Liu, M. Lin, X.W. Zhou, L. Zhao, A.L. Ning, and S.M. Zeng, Reprecipitation behavior in Al–Cu binary alloy after severe plastic deformation-induced dissolution of θ′ particles, *Mater. Sci. Eng. A*, 546(2012), p. 26.

[24] Y.J. Guo, G.W. Li, H.Y. Jin, Z.Q. Shi, and G.J. Qia, Intermetallic phase formation in diffusion-bonded Cu/Al laminates, *J. Mater. Sci.*, 46(2011), No. 8, p. 2467.

[25] Z.K. Liu and Y.A. Chang, Thermodynamic assessment of the Al–Fe–Si system, *Metall. Mater. Trans. A*, 30(1999), No. 4, p. 1081.

[26] Y.P. Xie, Z.Y. Wang, and Z.F. Hou, The phase stability and elastic properties of $MgZn_2$ and Mg_4Zn_7 in Mg–Zn alloys, *Scripta Mater.*, 68(2013), No. 7, p. 495.

[27] R. Kapoor, A. Sarkar, R. Yogi, S.K. Shekhawat, I. Samajdar, and J.K. Chakravartty, Softening of Al during multi-axial forging in a channel die, *Mater. Sci. Eng. A*, 560(2013), p. 404.

[28] J. Gubicza, N.Q. Chinh, G. Krállics, I. Schiller, and T. Ungár, Microstructure of ultrafine-grained fcc metals produced by severe plastic deformation, *Curr. Appl Phys.*, 6(2006), No. 2, p. 194.

[29] I. Sabirov, M.Y. Murashkin, and R.Z. Valiev, Nanostructured aluminium alloys produced by severe plastic deformation: New horizons in development, *Mater. Sci. Eng. A*, 560(2013), p. 1.

[30] T. Sakai, A. Belyakov, R. Kaibyshev, H. Miura, and J.J. Jonas, Dynamic and post-dynamic recrystallization under hot, cold and severe plastic deformation conditions, *Prog. Mater. Sci.*, 60(2014), p. 130.

[31] N. Kamikawa, X.X. Huang, N. Tsuji, and N. Hansen, Strengthening mechanisms in nanostructured high-purity aluminium deformed to high strain and annealed, *Acta Mater.*, 57(2009), No. 14, p. 4198.

[32] M.M. El-Rayes and E.A. El-Danaf, The influence of multi-pass friction stir processing on the microstructural and mechanical properties of Aluminum Alloy 6082, *J. Mater. Process. Technol.*, 212(2012), No. 5, p. 1157.

[33] I.S. Lee, P.W. Kao, and N.J. Ho, Microstructure and mechanical properties of Al–Fe *in situ* nanocomposite produced by friction stir processing, *Intermetallics*, 16(2008), No. 9, p. 1104.